Widely tunable thermo-optic plasmonic bandpass filter

Jongwon Lee and Mikhail A. Belkin

Citation: Applied Physics Letters **103**, 181115 (2013); doi: 10.1063/1.4828500
View online: http://dx.doi.org/10.1063/1.4828500
View Table of Contents: http://scitation.aip.org/content/aip/journal/apl/103/18?ver=pdfcov
Published by the AIP Publishing

Widely tunable thermo-optic plasmonic bandpass filter

Jongwon Lee and Mikhail A. Belkin[a)]
Department of Electrical and Computer Engineering, University of Texas at Austin, Austin, Texas 78758, USA

(Received 6 September 2013; accepted 16 October 2013; published online 30 October 2013)

We report thermally tunable optical bandpass filters based on long-range surface plasmon polariton waveguides. A thin gold stripe in the waveguide core is surrounded by dielectric layers with dissimilar refractive index dispersions and dissimilar thermo-optic coefficients. High filter transmission is achieved for a wavelength at which the refractive indices of the upper and lower cladding layers are identical, and this spectral point may be changed by varying the filter temperature. Experimentally, over 220 nm of bandpass tuning is achieved around 1550 nm wavelength by varying the device temperature from 19 to 27 °C. © *2013 AIP Publishing LLC*. [http://dx.doi.org/10.1063/1.4828500]

Compact and widely tunable monolithic optical filters are desirable for a variety of applications, such as spectroscopy, laser emission tuning, and telecommunications. The operating principle of compact monolithic photonic filters, such as Mach–Zehnder interferometers, Bragg reflectors, microresonator filters, and distributed feedback lasers, relies on light reflection and interference phenomena.[1,2] As a result, a change in the dielectric constant of a filter medium results in the shift in bandpass wavelength according to the equation

$$\lambda_1/n_1 = \lambda_2/n_2, \tag{1}$$

where λ_1 and λ_2 are the two device operating wavelengths that correspond to the two values of the refractive index of the device medium, n_1 and n_2. Since the relative refractive index variation in transparent dielectrics is limited to $\leq 1\%$ for thermo-optic and electro-optic materials and $\leq 15\%$ for liquid crystals, the tuning range of these devices is limited. In order to achieve broader tuning range, many approaches have been proposed using mechanical and micromechanical elements,[2,3] acousto-optic modulation,[4] and employing coupled-cavities or multi-section filters.[5–7] However, all of these approaches are complex and difficult to miniaturize. Graphene has been suggested as a suitable material for widely tunable filters in mid-infrared and terahertz range[8,9] although low-loss graphene filters are yet to be demonstrated.

Our group has recently demonstrated that unique properties of long-range surface plasmon-polaritons (LR SPP) modes may be used to create optical bandpass filters with very wide tuning range.[10] The proof-of-concept demonstration of the filter operation in Ref. 10 was carried out using a set of refractive index matching fluids. Here we report a thermo-optic solid-state LR SPP bandpass filter which provides over 220 nm of bandpass tuning around 1550 nm wavelength for a temperature variation of only 8 °C.

The LR SPP is a transverse magnetic (TM) polarized optical surface wave that can exist in a sufficiently thin metal film or stripe embedded in dielectrics with similar refractive indices above (n_t) and below (n_b) the metal.[11–14] An example of the LR SPP mode is shown in Fig. 1(a) for the waveguide configuration used in our experiment. Physically LR SPP is associated with coupling of the two surface plasmon polaritons (SPP) at the upper and lower interfaces between metal and dielectric. LR SPP waveguides may have optical propagation losses of only a few dB/cm at $\lambda = 1.55\ \mu$m (Ref. 15) and even lower at longer wavelength due to improved optical properties of metals. We note that LR SPP mode is the only mode supported by this waveguide.[16,17] Figure 1(b) shows calculated LR SPP mode when the refractive indices of the dielectrics above and below the metal stripe are matched. The LR SPP mode is well-confined and well-matched with optical modes in fibers, leading to very low insertion loss of LR SPP waveguides in fiber-optic systems.[12,14–16,18–22] The insertion loss of the LR SPP waveguides will increase dramatically if the refractive indices n_t and n_b of the cladding dielectrics are even slightly mismatched due to the severe mode mismatch to optical fiber mode (see Figs. 1(c) and 2(a)).[10,16,19–23]

Propagation and coupling losses for a 4-mm-long, 2.7-μm-wide, and 20-nm-thick gold stripe waveguide integrated with single mode optical fibers (SMF-28) for end-fire mode coupling are analyzed in Figure 2(a) for 1.43 μm wavelength. The top panel in Fig. 2(a) shows the calculated mode power attenuation (MPA) for the LR SPP mode and the coupling loss for SMF-28 to LR SPP mode coupling for one facet as a function of the refractive index mismatch ($\delta n = n_t$-n_b) between the top and bottom dielectrics. The bottom panel in Fig. 2(a) shows the total insertion loss as a function of the refractive index mismatch ($\delta n = n_t$-n_b) between the top and bottom dielectrics. For numerical calculations, a commercial finite-element package (COMSOL 4.3) was used to solve LR SPP mode's complex effective index n_{eff}. The mode power attenuation was determined from the imaginary part of the n_{eff}, and the mode coupling loss was calculated using a mode overlap integral between the LR SPP mode and the SMF mode modeled as a Gaussian distribution centered on the waveguide.[24] The total insertion loss was then calculated by combining the power attenuation during the propagation and the LR SPP mode coupling and out-coupling loss at the input and output facets. As shown in top panel of Fig. 2(a), the MPA decreases gradually as δn increases because the LR

[a)]Author to whom correspondence should be addressed. Electronic mail: mbelkin@ece.utexas.edu

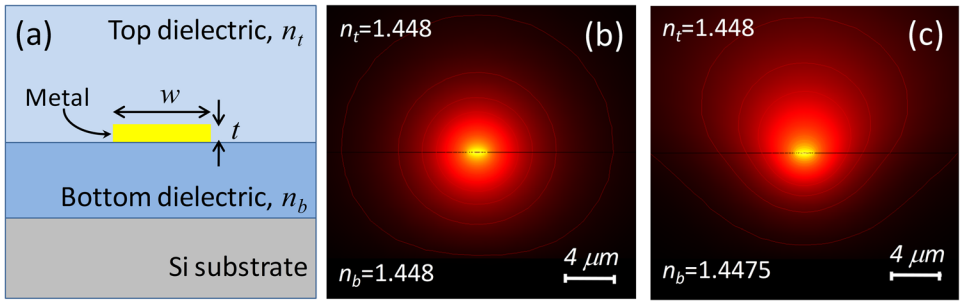

FIG. 1. (a) Cross-sectional view of LR SPP waveguide used in our experiments. The waveguide is fabricated on a Si substrate with 15 -μm-thick layer of thermally grown SiO_2 served as bottom dielectric n_b. The waveguide metal core is made of gold with $t = 20$ nm thickness and $w = 2.7$ μm width. A 34-μm-thick layer of a thermo-optic polymer is used as top dielectric n_t. (b) Calculated intensity profile of a LR SPP mode at $\lambda = 1.428$ μm for the structure in (a) when $\delta n = n_t\text{-}n_b = 0$. (c) Same as (b) for the case when $\delta n = n_t\text{-}n_b = 0.0005$. Slight LR SPP mode asymmetry in (b) is due to the presence of a Si substrate.

SPP mode is less confined to the metal stripe. On the other hand, the mode coupling loss of LR SPP to the SMF mode increases sharply as δn increases due to the LR SPP mode distortion (see Fig. 1(c)), and this coupling loss dominantly contributes to the total optical loss. As a result, the total insertion loss increases dramatically as δn increases, and the maximum transmission will be given when the refractive indices of the top and bottom dielectrics are matched (see the bottom panel of Fig. 2(a)).

Our filter design is based on integration of a thin metal film between two dielectrics with *dissimilar* refractive index dispersion. In this configuration, the LR SPP waveguide will only have low insertion loss (high transmission) at a wavelength for which the refractive indices of the top and bottom dielectrics are the same, leading to a bandpass filter as shown in Fig. 2(b). To build a temperature tunable LR SPP bandpass filter, we use a thermo-optic polymer (ZPU-1446 from ChemOptics, Inc.) with thermo-optic coefficient of -1.86×10^{-4} K^{-1} as our top cladding layer and an optically thick layer of SiO_2 which has relatively small thermo-optic coefficient of only 10^{-5} K^{-1} (Ref. 23) as the bottom cladding layer as shown in Fig. 1(a). The top panel in Fig. 2(b) shows the refractive indices of ZPU-1446 and SiO_2 at different temperatures as a function of wavelength. Due to an extreme sensitivity of LR SPP waveguide insertion loss on δn, high filter transmission occurs only at wavelength λ for which $n_t(\lambda) \approx n_b(\lambda)$. A small change in the refractive index of the top dielectric (δn_t) by changing temperature may now be translated into the large shift in the LR SPP filter bandpass ($\delta\lambda$) as shown in the bottom panel in Fig. 2(b). The filter tuning is determined by the equation[10]

$$\delta\lambda \approx \delta n_t \Big/ \left(\frac{dn_t}{d\lambda} - \frac{dn_b}{d\lambda}\right), \tag{2}$$

where $dn_t/d\lambda$ and $dn_b/d\lambda$ are the refractive index dispersion of n_t and n_b, and δn_t is the refractive index variation in the top dielectric due to temperature change. Here we assume that only the refractive index of the top dielectric is affected by temperature in agreement with the data in the top panel in Fig. 2(b).

The LR SPP waveguide was fabricated on a Silicon wafer with 15 μm-thick layer of thermally grown SiO_2. The 20-nm-thick and 2.7-μm-wide metal stripe was fabricated by sequential processes of an image reversal photolithography with an AZ5214E photoresist, a gold coating by electron beam evaporation, and the lift-off process. A 34-μm-thick layer of UV-curable ZPU-1446 thermo-optic polymer was

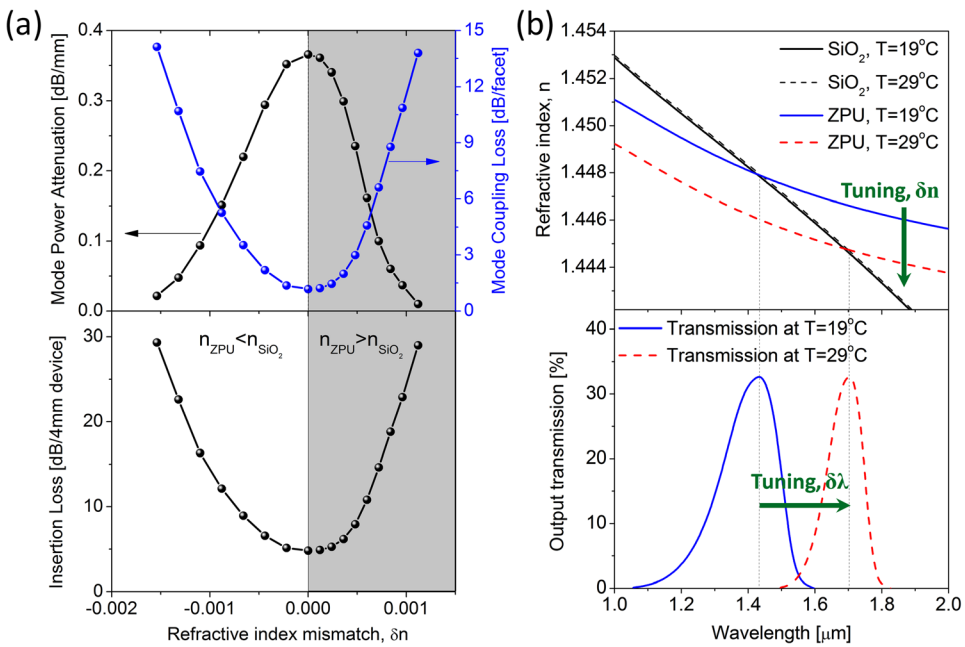

FIG. 2. (a) Top panel: calculation of the mode power attenuation (left axis) and modal coupling loss (right axis) as a function of $\delta n = n_t\text{-}n_b$ for the LR SPP waveguide described in Fig. 1 at $\lambda = 1.428$ μm. Bottom panel: calculation of the total insertion loss for a 4-mm-long device. The insertion loss increases sharply as the refractive index mismatch increases. (b) The principle of the LR SPP thermo-optic filter operation. Top panel: refractive index dispersion curves for the bottom dielectric SiO_2 and the top dielectric ZPU at 19 °C and 29 °C. Bottom panel: calculated optical throughput of the 4-mm-long LR SPP filter at 19 °C and 29 °C.

spin-coated on top of the structure and then cured in an UV light irradiation chamber with an optical power density of 15 mW/cm^2 for 10 min in nitrogen atmosphere. Finally the wafer was cleaved to form a 4-mm-long waveguide section.

The experimental configuration used to demonstrate the LR SPP filter operation is depicted in Fig. 3. The filter was mounted on a temperature-controllable thermo-electric plate and the input and output SMF-28 optical fibers were mounted on three-axis auto-alignment system on left and right side of the sample. A broadband source ($\lambda = 400$ nm-2000 nm, SuperK) coupled to a SMF was used to excite the LR SPP mode via end-fire coupling of light. It should be noted that radiation from the broadband source was unpolarized and only TM-polarized light can couple to LR SPP. The output light was collected by SMF coupled to an optical spectrum analyzer. The positions of the input and output fiber were adjusted to maximize the transmitted output power. The transmitted broadband output spectrum was recorded and normalized to TM-polarized portion of the input from the SMF. The filter temperature was varied from 19 °C to 27 °C.

Top panel of Fig. 4 shows the refractive index dispersion curves for the SiO_2 bottom dielectric at the extreme operating temperatures and the top ZPU polymer dielectric layer at the five different temperatures within the temperature variation range. The ZPU polymer has a much larger thermo-optic coefficient than SiO_2 and changes its refractive index with temperature significantly, while the refractive index of SiO_2 stays virtually constant. For each temperature, the refractive index dispersion curve of the ZPU polymer intersects that of SiO_2 at a different wavelength. The bottom panel of Fig. 4 shows calculated and experimental power transmission spectra through the 4 mm-long LR SPP filter. As expected, the filter transmission is maximal at wavelengths for which the indices of the top and bottom dielectrics are matched and drops as off away from the matching point. Simulated transmission spectra were calculated using the refractive index dispersion data for each temperature and assuming the LR SPP mode is coupled from and out-coupled into a SMF-28 fiber with the insertion loss given in Fig. 2(a). Experimentally, a temperature variation of 8 °C translates into a wavelength tuning range of $\delta\lambda \approx 220$ nm ($\lambda = 1430$–1650 nm) with a

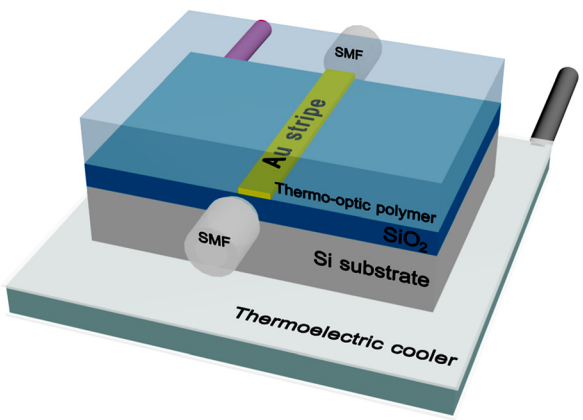

FIG. 3. The LR SPP tunable bandpass filter structure and the experimental configuration. Single mode fibers were used for light coupling and out-coupling.

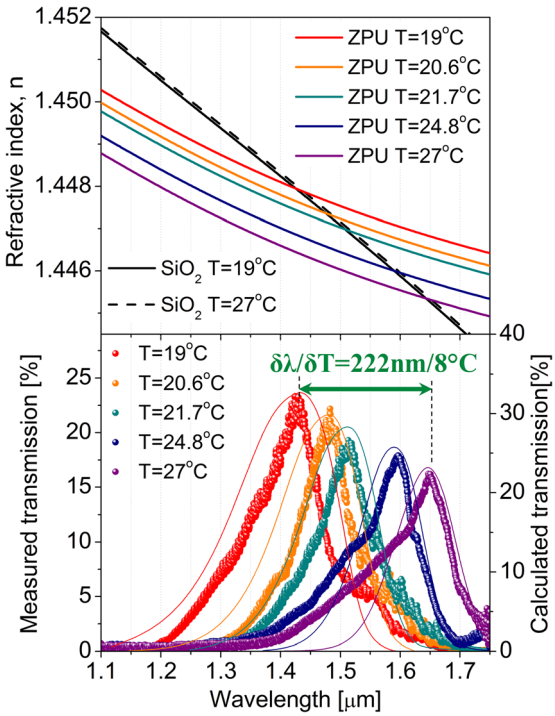

FIG. 4. Top panel: refractive index dispersion curves for SiO_2 and ZPU-1446 polymer at different operating temperatures. Bottom panel: calculation (thin line) and experimental data (circles) for the filter transmission at five different temperatures.

28 nm/°C of temperature sensitivity. We note that the gold stripe width for the LR SPP waveguide ($W = 2.7\ \mu m$) was chosen to provide the best spatial overlap between the LP SPP mode and the SMF-28 fiber mode at 1.43 μm wavelength. As a result, our filter displays the highest peak transmission at $T = 19$ °C when the bandpass is centered at 1.43 μm. The peak transmission drops at higher temperatures as the filter bandpass shifts to longer wavelengths. This trend is observed both experimentally and in simulations as seen in Fig. 4.

Further work is planned to reduce the filter transmission linewidth, which could be achieved, e.g., by stacking multiple LR SPP filters and by tailoring width, thickness, and material of the metal stripe to make LR SPP mode more sensitive to the refractive index mismatch between the top and bottom dielectrics. We note that LR SPP filters are expected to operate equally well in mid-infrared spectral range (3–15 μm), which is very important for spectroscopy, as long as proper metal geometries and dielectric claddings are chosen.

In summary, we have demonstrated a thermally-tunable optical bandpass filter with tuning range of $\delta\lambda \approx 220$ nm around 1550 nm wavelength based on LR SPP waveguide that uses a thermo-optic polymer as top dielectric. The filter design allows one to translate a small refractive index tuning range of the top dielectric into a large filter bandpass tuning range. The filters are simple in fabrication and may be integrated with fiber-optic and semiconductor laser systems to create optical components with widely tunable spectral response. The broad tuning range of these devices is appealing, in particular, for tunable laser systems, spectroscopic applications, and imaging.

This work was supported by the Air Force Office of Scientific Research under Contact No. FA9550-10-1-0076. Sample fabrication was carried out in the Microelectronics Research Center at the University of Texas at Austin, which is a member of the National Nanotechnology Infrastructure Network. The authors are thankful to Professor Ray T. Chen for providing an access to his laboratory equipment.

[1]G. P. Agrawal, *Lightwave Technology: Components and Devices* (John Wiley & Sons, New York, 2004).
[2]O. Solgaard, *Photonic Microsystems* (Springer, New York, 2009).
[3]C. Ye, *Tunable External Cavity Diode Lasers* (World Scientific Publishing, Singapore, 2004).
[4]L. Bei, G. I. Dennis, H. M. Miller, T. W. Spaine, and J. W. Carnahan, Prog. Quantum Electron. **28**, 67 (2004).
[5]J. W. Evans, J. Opt. Soc. Am. **39**, 229 (1949).
[6]I. Šolc, J. Opt. Soc. Am. **55**, 621 (1965).
[7]W. T. Tsang, N. A. Olsson, and R. A. Logan, Appl. Phys. Lett. **42**, 650 (1983).
[8]M. Liu, X. B. Yin, E. Ulin-Avila, B. S. Geng, T. Zentgraf, L. Ju, F. Wang, and X. Zhang, Nature **474**(7349), 64 (2011).
[9]B. Sensale-Rodriguez, T. Fang, R. Yan, M. M. Kelly, D. Jena, L. Liu, and H. Xing, Appl. Phys. Lett. **99**, 113104 (2011).
[10]J. Lee, F. Lu, and M. A. Belkin, Opt. Lett. **36**, 3744 (2011).
[11]M. Fukui, V. So, and R. Normandin, Phys. Status Solidi B **91**, K61 (1979).
[12]D. Sarid, Phys. Rev. Lett. **47**, 1927 (1981).
[13]H. Dohi, Y. Kuwamura, M. Fukui, and O. Tada, J. Phys. Soc. Jpn. **53**, 2828 (1984).
[14]R. Charbonneau, P. Berini, E. Berolo, and E. Lisicka-Shrzek, Opt. Lett. **25**, 844 (2000).
[15]A. Boltasseva, T. Nikolajsen, K. Leosson, K. Kjaer, M. S. Larsen, and S. I. Bozhevolnyi, J. Lightwave Technol. **23**, 413 (2005).
[16]F. Yang, J. R. Sambles, and G. W. Bradberry, Phys. Rev. B **44**, 5855 (1991).
[17]P. Berini, R. Charbonneau, S. Jette-Charbonneau, N. Lahoud, and G. Mattiussi, J. Appl. Phys. **101**, 113114 (2007).
[18]J. J. Ju, S. Park, M. Kim, J. T. Kim, S. K. Park, Y. J. Park, and M.-H. Lee, Appl. Phys. Lett. **91**, 171117 (2007).
[19]L. Wendler and R. Haupt, J. Appl. Phys. **59**, 3289 (1986).
[20]J. J. Burke, G. I. Stegeman, and T. Tamir, Phys. Rev. B **33**, 5186 (1986).
[21]P. Berini, Phys. Rev. B **63**, 125417 (2001).
[22]I. Breukelaar and P. Berini, J. Opt. Soc. Am. A **23**, 1971 (2006).
[23]E. D. Palik, *Handbook of Optical Constants of Solids* (Academic Press, San Diego, 1998).
[24]P. Berini, R. Charbonneau, N. Lahoud, and G. Mattiussi, J. Appl. Phys. **98**, 043109 (2005).